Quantitative phase analysis in electron holographic interferometry

Toyohiko Yatagai, Katsuyuki Ohmura, Shigeo Iwasaki, Shuji Hasegawa, Junji Endo, and Akira Tonomura

Holographic interferometry in an electron microscope and its phase analysis technique are described. The fringe scanning method is used to gain high sensitivity in phase detection. An example of measuring a magnetic field of a fine particle is presented. The measurement accuracy for median filtering is about 1/70 fringe corresponding to the magnetic flux sensitivity of 6×10^{-17} Wb. Noise reduction techniques are also discussed.

I. Introduction

Holography has been successfully used in an electron microscope since the field-emission electron microscope was developed.[1–3] This microscope differs from a conventional electron microscope in two respects: a field-emission electron gun provides a coherent electron beam and a Möllenstedt-type electron biprism is used as a wavefront beam splitter for recording holograms.

In an earlier stage of the electron holography technique, correction of spherical aberration in an electron optical system was a major objective to improve its spatial resolution.[4–6] Then a 3-D imaging technique, a phase-contrast method, and an interferometric technique[7] were discussed. Among applications of electron holography, electron holographic interferometry promises to make unique contributions. With it thickness variations and magnetic field distributions in a microscopic region can be detected.

To gain high sensitivity in interferometric phase measurement, the use of the optical phase amplification technique[8,9] was discussed to obtain tenfold amplification of the reconstructed phase by using higher diffraction orders.[7,10] Recently Takeda *et al.*, used the FFT method of subfringe analysis for electron holographic fringes.[11] They described phase variations much smaller than 2π that could be detected without recourse to optical reconstruction or optical interferometric measurements.

In this paper, using the fringe scanning technique for fringe analysis of an electron interference hologram is discussed. It gives us high sensitivity and high spatial resolution in phase measurement. The quantitative phase measurement technique in electron holographic interferometry is useful for magnetic field measurements in the microscopic region as well as for small thickness variation evaluation. We first present a brief review of electron holographic interferometry and then discuss the use of the fringe scanning technique.

Toyohiko Yatagai and K. Ohmura are with University of Tsukuba, Institute of Applied Physics, Tsukuba Science City, Ibaraki 305, Japan; S. Iwasaki is with National Research Laboratory for Metrology, Tsukuba Science City, Ibaraki 305, Japan; and the other authors are with Hitachi, Ltd., Advanced Research Laboratory, Kokubunji, Tokyo 185, Japan.

Received 23 June 1986.
0003-6935/87/020377-06$02.00/0.
© 1987 Optical Society of America.

II. Electron Holographic Interferometry

A. Electron Holography

A schematic diagram of an electron holographic system is shown in Fig. 1. A specimen is positioned in one-half of a collimated beam; the other half is used as the reference beam. An image of the specimen is formed through an objective lens. A Möllenstedt-type electron biprism is situated between the objective lens and the image plane. The Möllenstedt biprism is composed of a central thin wire and two ground-potential electrodes on both sides. Application of a positive electric potential to the wire makes the image and the reference beam overlap giving interference fringes. The interference fringe pattern is magnified by a magnification lens and recorded on film as an electron hologram.

By using an optical system an image of an electron hologram can be reconstructed, as shown in Fig. 2. A hologram is illuminated by a collimated monochromatic light. An electron objective lens has a very large spherical aberration, which limits the resolution of the

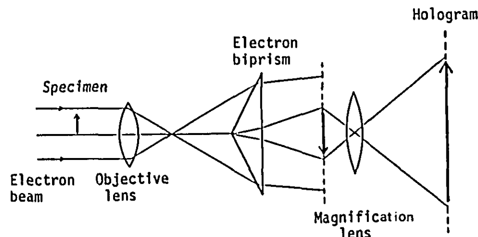

Fig. 1. Schematic diagram of an electron hologram recording.

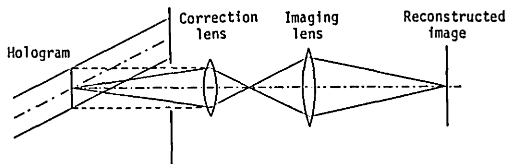

Fig. 2. Optical reconstruction system of an electron hologram. Phase difference amplification is done by using higher-order diffracted waves.

electron microscope. When this spherical aberration needs to be reduced, a correction lens is used in an optical reconstruction system to compensate the spherical aberration of the electron optics.

B. Phase in Reconstructed Image

In an optically reconstructed image, the phase of the transmitted electron beam is also reconstructed. Superimposing a plane reference wavefront on the reconstructed image gives an interference fringe pattern corresponding to the phase contours of the object. In an optical reconstruction system for the interference microscope based on the electron holography, two collimated laser beams coherent with each other illuminate a hologram, so that the plus Kth order and the minus Kth order reconstructed images make a phase-difference amplified interference pattern by a factor of $2K$. As described later, a combination of the first- and zero-order diffracted waves is used to obtain an interferogram without phase amplification.

The phase difference between an object beam and a reference beam is caused by two sources: thickness variation and magnetic flux. The effective refractive index n of a nonmagnetic specimen can be derived as

$$n = 1 + V_0/2\phi_0, \tag{1}$$

where V_0 is the mean potential of the specimen and ϕ_0 is the initial electron potential. Thus the phase change due to thickness variation d is given by

$$\Delta\phi = n \cdot d. \tag{2}$$

The phase difference resulting from the magnetic flux is described by

$$\Delta\phi = -2\pi \cdot e/h \cdot \int B_n dS, \tag{3}$$

where e is the electron charge and h is Planck's constant. According to Eq. (3), a 2π phase difference or one fringe in an interferogram corresponds to a closed magnetic flux of $h/e = 4 \times 10^{-15}$ Wb. This value represents high sensitivity compared with that of any other conventional field-measurement techniques.

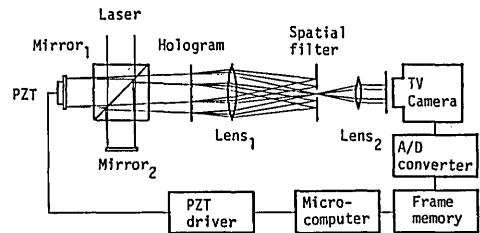

Fig. 3. Schematic diagram of hologram reconstruction and fringe analysis.

III. Phase Analysis

A. Procedure and Experimental Apparatus

Figure 3 is a schematic of the setup for reconstructing an electron hologram and making the fringe scanning phase detection of the reconstructed image. In the first experiment presented, the zero-order diffracted wave is used as the reference beam and so the plus first-order and the zero-order diffracted waves are superimposed to obtain an interference fringe pattern. One of the reconstructed beams is phase shifted with a PZT driven modulation mirror, so that the phase of the interference fringe pattern is adjusted to make phase-sensitive detection. When making phase-difference amplification of the reconstructed image, we superimpose the plus and the minus first orders of diffraction to obtain an interference fringe pattern with the twice-amplified phase distribution.

The interference fringe pattern is detected with a high-resolution low-distortion TV camera and is stored in a frame memory. Fringe data are transferred to a minicomputer. The PZT transducer is controlled by a minicomputer via a D–A converter.

B. Algorithm

Let us suppose that the interference fringe pattern with the modulated reference phase δ_n can be written as

$$f(x,y,\delta_n) = a(x,y) + b(x,y) \cos[\phi(x,y) + \delta_n], \tag{4}$$

where $\phi(x,y)$ is the phase to be evaluated and $a(x,y)$ and $b(x,y)$ are the average fringe intensity and the fringe contrast, respectively. In the fringe scanning method, one of the mirrors is stepwise moved through half of the wavelength so that the relative phase δ_n of the interferogram is changed:

$$\delta_n = 2\pi/N \qquad (N = 1,2,\ldots,N-1), \tag{5}$$

where N denotes the number of mirror movements. The irradiance at each point in the interference pattern goes through one cycle of periodic variation. The computer determines a best-fit sinusoidal function for the irradiance vs the amount of phase shift at each point of the interference pattern. The phase of the best-fit function is a direct measure of the test wavefront.

According to the fringe scanning phase detection principle,[12] summations with sinusoidal weights

$$c(x,y) = \sum_{n=0}^{N-1} f(x,y,\delta_n) \cos 2\pi n/N, \quad (6)$$

$$s(x,y) = \sum_{n=0}^{N-1} f(x,y,\delta_n) \sin 2\pi n/N \quad (7)$$

are calculated to extract the sinusoidal parts of the intensity variation. The phase of the interferograms is given by

$$\phi(x,y) = \tan^{-1} \frac{s(x,y)}{c(x,y)} . \quad (8)$$

The calculated arctangent values are wrapped between $\pm\pi$ rad. The unwrapped phase value gives the correct shape corresponding to the phase profile.

C. Data Analysis Software System

To make automatic data acquisition and phase analysis, we developed a software system whose flow diagram is shown in Fig. 4. If necessary, prior to entering a main processing routine, preprocessing procedures are performed. The preprocessing step includes the piezoelectric translator calibration. The nonlinear characteristic of the piezoelectric translator is measured. The coefficients of the calibration quadratic curve of translation vs the input voltage are evaluated.[13] By using these evaluated coefficients, a corrected voltage is available for the phase-shifting procedures.

In the first processing step, a series of interferograms with different reference phases and the first-order reconstructed image without the reference beam are stored in a computer memory. This first-order reconstructed image is used to reduce background noise in the interferograms in the next step. Noise reduction procedures are performed in the second step. TV frame averaging, unweighted local averaging, and median filtering are used to reduce statistical noise in interferograms. To obtain enhanced fringe contrast and to reduce the background noise, the first-order reconstructed image is subtracted from the interferogram data. The phase of the interferogram is calculated according to Eq. (8). The computation of phase by any inverse trigonometric function only provides phase principal values between $\pm\pi$ rad. In the third step, this phase unwrapping is performed. In the postprocessing step, the aberration of the optical interferometer and the tilt phase term are subtracted from the unwrapped phase data. Finally, calculated phase data are displayed in an arbitrary format.

D. Noise Reduction

The noise sources to be considered in electron holographic interferometry are (1) phase irregularity in a carbon film base which supports the specimen, (2) speckle noise caused by dust and such in the optical reconstruction system, (3) thickness irregularity and scattering of a hologram, and (4) electronic statistical noise: shot noise and thermal noise in a TV camera.

In spatial noise due to the first three sources, we use noise reduction techniques by digital image processing

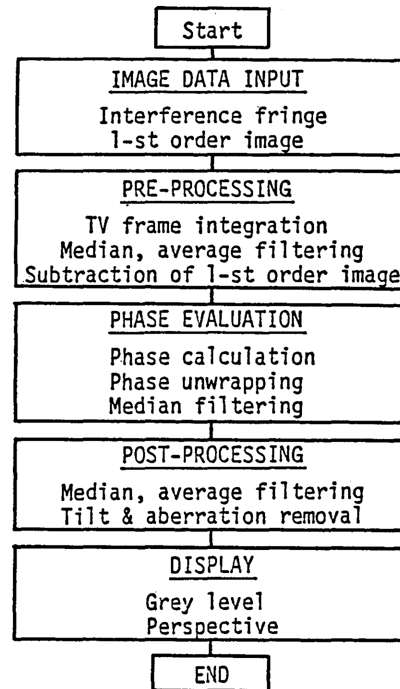

Fig. 4. Flow diagram of the software system for automatic data acquisition and phase analysis.

including local averaging, median windowing, and some spatial filtering. In particular, median window filtering is powerful in reducing salt-and-pepper spatial noise without reducing spatial resolution. Spatially independent noise such as salt-and-pepper noise in the analyzed phase distribution is serious enough to perform phase unwrapping, resulting in fatal errors near the phase discontinuity area. TV frame averaging in time provides for reduction of the statistical noise from the fourth statistical source above.

In addition to the technique mentioned above, speckle noise due to the reconstructed optical system could be reduced by using incoherent illumination to decrease the effects of diffraction patterns from dust and by using a liquid gate method to compensate phase irregularity in a hologram surface.

IV. Experimental

As shown in Fig. 3, the experimental system is divided into two parts: optical and electronic. The optical system used is a Twyman-Green interferometer with a reference phase-modulation function. The fringe analysis system consists of high-resolution TV camera (Hamamatsu C1000), frame memory, piezoelectric translator and its driver, and a DEC LSI-11/23 minicomputer system. The video signal is converted to an 8-bit digital signal and stored in the frame memory of a Hamamatsu C1901 with a 16-bit resolution. Because of the 16-bit resolution in the intensity range, 256 frames maximum can be accumulated in the frame memory to reduce statistical noise in the video signal. A piezoelectric translator (Burleigh PZ-91) makes the phase modulation. A programmable high voltage sup-

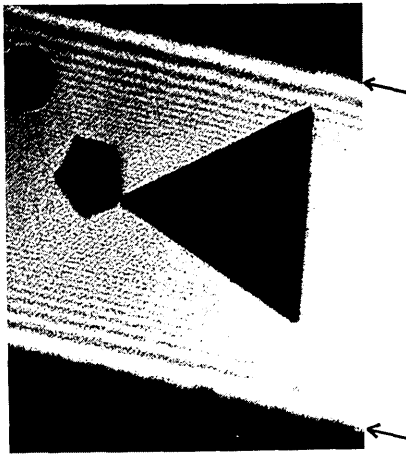

Fig. 5. Magnified version of an electron hologram. Holographic carrier fringes are observed between the arrows.

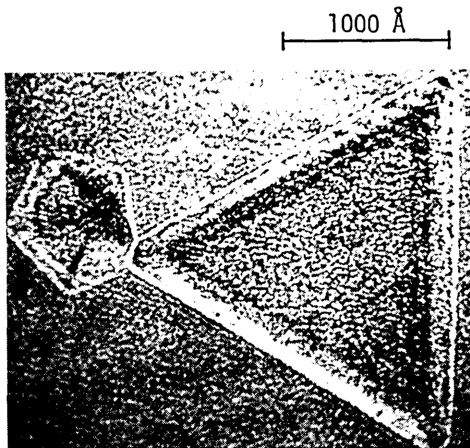

Fig. 6. Reconstructed image of a cobalt particle.

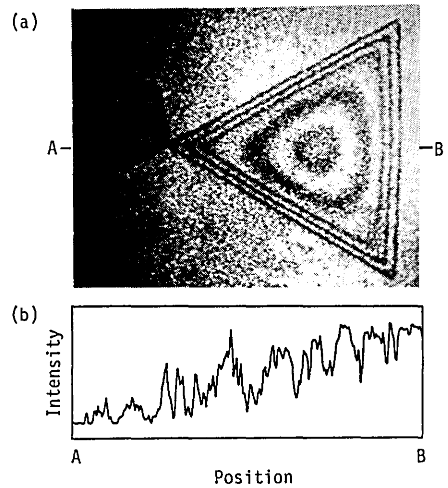

Fig. 7. Interference micrograph of (a) magnetic particle and (b) its fringe intensity profile along a central cross section.

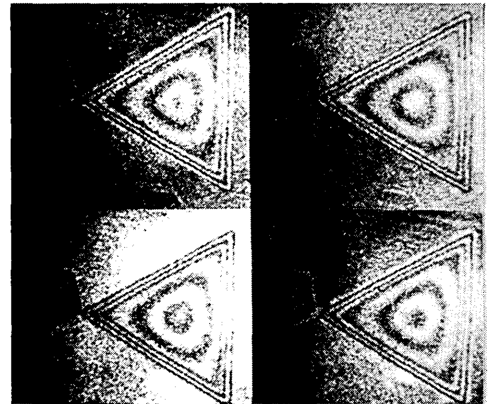

Fig. 8. Interferometric micrograms with different reference phases.

ply is developed in which a 12-bit Datel HK12BGC D–A converter generates the reference signal.

Electron holograms are recorded in a 125-kV field-emission electron microscope. The interference fringes are magnified 30,000 times in the electron microscope and recorded on Kodak 4489 electron microscope film as a hologram. The carrier frequency is 20 lines/mm. A magnified version of an electron hologram is shown in Fig. 5. The specimen is a magnetic cobalt particle mounted on a carbon thin film. Between the arrows indicated in the figure two electron beams are the overlapped and interferometric fringes obtained. The number of holographic carrier fringes in this area is ~250.

Figure 6 shows a reconstructed image of a cobalt particle. The image is reconstructed without a reference beam in the optical system shown in Fig. 3. The size of the particle is ~2000 Å. The speckle noise is obvious in the reconstructed image.

The interferometric fringe pattern is shown in Fig. 7(a), which is obtained by superimposing the first-order diffracted wave and the zero order from the hologram of Fig. 5. An intensity profile along a central cross section is shown in Fig. 7(b). The interferogram has a salt-and-peppery appearance due to the randomness of the speckle. Five interference fringes are observed in the reconstructed image. Since the particle is verified to be planar and triangular by another method, the outer three fringes are due to the thickness variation and the inner two fringes correspond to magnetic flux inside the particle.

Figure 8 shows interferograms with $\pi/2$ reference phase difference. The principal values of the phase are calculated according to Eq. (8). The calculated phase distribution is shown in Fig. 9(a). Phase irregularity from speckle noise is observed in the phase profile along a central cross section shown in Fig. 9(b). By using a 3×3 pixel median filtering window, this type of phase irregularity is reduced as shown in Fig. 10.

Figure 11 shows a grey level version of an unwrapped phase distribution and its profile along a central cross section. In the unwrapped phase distribution, a tilted phase term due to optical misalignment or a background phase is compensated by using a least-squares-estimation method. A 3-D plot of the unwrapped phase distribution is shown in Fig. 12.

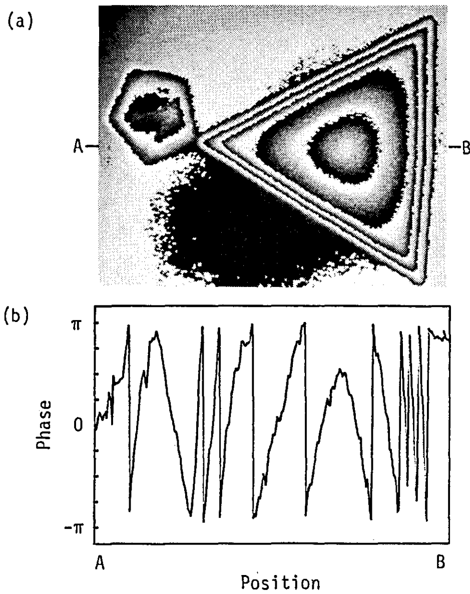

Fig. 9. Calculated phase distribution: (a) wrapped phase and (b) its profile along a central cross section.

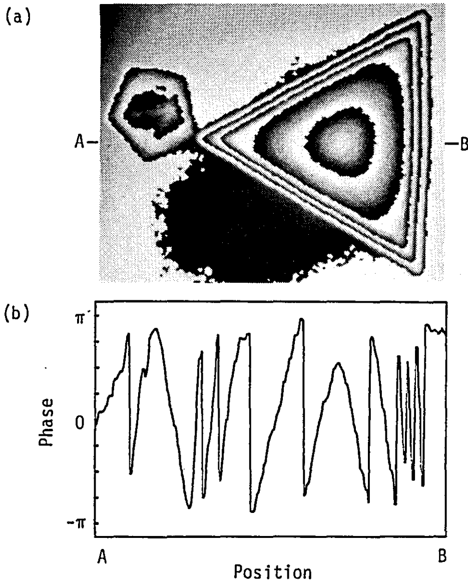

Fig. 10. Result of median window filtering of phase distribution shown in Fig. 9.

To evaluate the measurement noise or the accuracy limit of the measurement, variance of the calculated phase data is estimated. Figure 13 shows the phase profiles for evaluation of measurement noise. The phase profile (a) in Fig. 13 is an unfiltered phase obtained by unwrapping the profile shown in Fig. 9(b). Median filtering of the phase profile (a) gives the phase profile (b), which corresponds to Fig. 11(b). The phase profile (c) is the result of twice-applied median filtering of the phase profile (b). The noise levels or accuracy limits (a), (b), and (c) are estimated to be 1/50, 1/60, and 1/70 fringe spacing, respectively.

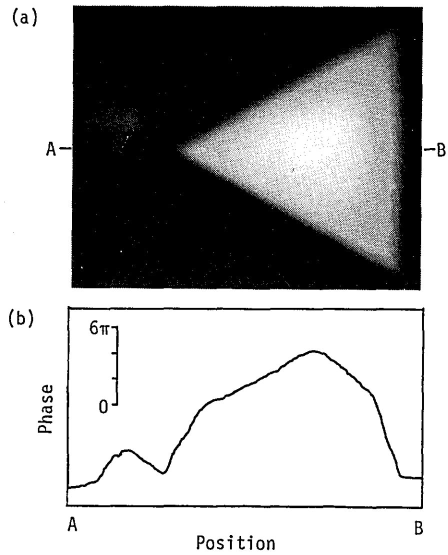

Fig. 11. (a) Unwrapped phase distribution and (b) its profile along a central cross section.

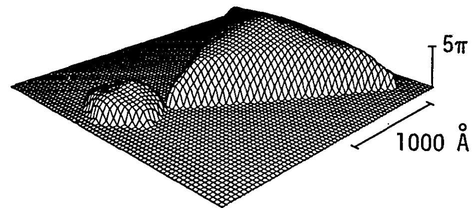

Fig. 12. Three-dimensional plot of the phase distribution shown in Fig. 11.

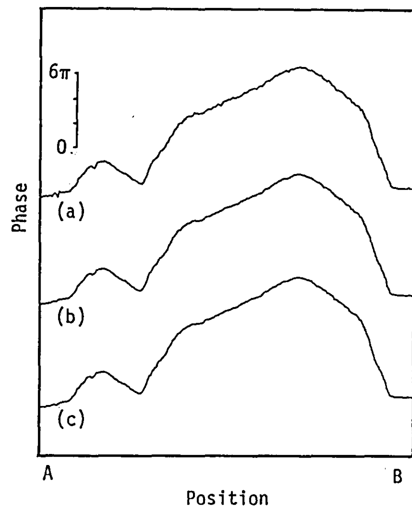

Fig. 13. Phase profiles in linear parts of Figs. 9(b) and 10(b). Evaluated phase variances are 1/50 and 1/70 fringes, respectively.

In the phase amplification case, higher diffraction orders are used to make interference fringes. If the plus first order and the minus first order in reconstruction are used, the phase of the interferogram is magnified by a factor of 2.

V. Concluding Remarks

We have described the importance of the phase-sensitive detection method in the electron holographic microscope. The fringe scanning phase-detection technique is applied to a phase-amplified holographic fringe pattern recorded with magnetic field distribution. In the present experiment the measurement accuracy is from about 1/50 to 1/70 fringe, depending on filtering. This corresponds to a magnetic flux sensitivity of from 6×10^{-17} to 8×10^{-17} Wb. Using higher diffraction orders, a noise reduction technique, and a more stable interferometer, we expect to obtain much higher accuracy of the present situation. According to theoretical considerations 1/1000-fringe accuracy for the fringe scanning algorithm is expected in the ideal case.

This paper is based on one presented at the OSA Topical Meeting on Holography, 31 Mar.–2 Apr. 1986.

References

1. A. Tonomura, J. Endo, and T. Matsuda, "An Application of Electron Holography to Interference Microscopy," Optik **53**, 143 (1979).
2. A. Tonomura, *et al.*, "Electron Holography Technique for Investigating Thin Ferromagnetic Films," Phys. Rev. B **25**, 6799 (1981).
3. A. Tonomura, "Application of Electron Holography Using a Field-Emission Electron Microscope," J. Electron Microsc. **33**, 101 (1984).
4. D. Gabor, "Microscopy by Reconstructed Wave Fronts," Proc. Soc. London Ser. A **197**, 454 (1949).
5. D. Gabor, "Microscopy by Reconstructed Wavefronts: II," Proc. Phys. Soc. B **64**, 449 (1951).
6. A. Tonomura, T. Matsuda, and J. Endo, Jpn. J. Appl. Phys. **18**, 1373 (1979).
7. J. Endo, T. Matsuda, and A. Tonomura, "Interference Electron Microscopy by Means of Holography," Jpn. J. Appl. Phys. **18**, 2291 (1979).
8. K. Matsumoto and M. Takashima, "Phase-Difference Amplification by Nonlinear Holograms," J. Opt. Soc. Am. **60**, 30 (1970).
9. K. Matsuda, C. H. Freund, and P. Hariharan, "Phase-Difference Amplification Using Longitudinally Reversed Shearing Interferometry: An Experimental Study," Appl. Opt. **20**, 2763 (1981).
10. J. Endo, T. Kawasaki, T. Matsuda, N. Osakabe, and A. Tonomura, "Sensitivity Improvement in Electron Holographic Interferometry," in *Conference Digest, Thirteenth Congress of the International Commission for Optics*, Sapporo (1984), p. 480.
11. M. Takeda and Q-S. Ru, "Computer-Based Highly Sensitive Electron-Wave Interferometry," Appl. Opt. **24**, 3068 (1985).
12. J. H. Bruning, D. R. Herriot, D. P. Rosenfeld, A. D. White, and D. J. Brangaccio, "Digital Wavefront Measuring Interferometer for Testing Optical Surfaces and Lenses," Appl. Opt. **13**, 2693 (1974).
13. T. Yatagai and T. Kanou, "Aspherical Surface Testing with Shearing Interferometer Using Fringe Scanning Detection Method," Opt. Eng. **23**, 357 (1984).

Books *continued from page 376*

Physics of New Laser Sources. Edited by N. ABRAHAM, F. ARECCHI, A. MOORADIAN, and A. SONA. Plenum Press, New York, 1986. 460 pp. $75.00.

This book is a collection of articles based on the lectures and seminars presented at the NATO Advanced Study group of the Europhysics School of Quantum Electronics which was held at Centro I Cappuccini, San Miniato, Tuscany, 11–21 July 1984. The subject matter of the articles provides updated information for young researchers and advanced graduate students who are already engaged in the area of lasers or for those wishing to enter this area. The topics covered are also likely to be of interest to both scientists from industrial laboratories as well those in the academic community.

Abraham, Arecchi, Mooradian, and Sona assembled at the meeting some of the world's pioneers in the laser field to lecture on the developments of new laser sources currently available up to 1984. The topics reviewed in this book are excimer, alexandrite, dye, pulse compression, semiconductor, and C^3 lasers, free electron lasers, synchrotron radiation, and Er lasers to name a few. Articles on phase conjugation and stimulated Raman scattering are also present. Two important laser sources not covered in the text in any great depth are other tunable solid-state lasers based on Cr^+, V^+, and Ti^+ ions and the supercontinuum laser.

This book can help serve as a reference for the end laser user community who needs to be informed about the state of the art of the future laser generation and how to explore uses of these new laser sources in future applications.

R. R. ALFANO

Laser Processing and Diagnostics: Proceedings of an International Conference. Edited by D. BAUERLE Springer-Verlag, New York, 1984. 551 pp. $34.00.

Laser Processing and Diagnostics is the proceedings of an international conference held in Linz, Austria, 15–19 July 1984. This interdisciplinary conference was devoted to fundamental aspects and applications of laser processing. The invited and contributed papers contained in the proceedings volume are compiled into five separate complementary chapters on topics ranging from basic studies of photophysical and photochemical processes at surfaces to photo-assisted semiconductor processing and laser diagnostics of gas phase and surface processes. The primary emphasis of the book is in the area of laser processing of electronic materials. The papers are generally well written, and the editor has organized them into a coherent and logical format. Also, an extensive subject index has been compiled; this is a valuable addition that is often lacking in conference proceedings.

The first chapter is devoted to fundamental aspects of the interaction between laser radiation and solid surfaces and applications of transient heating methods for processing of electronic materials. The chapter contains fifteen papers which address issues relating to laser-induced phase transformations in Si, Ge, Te, GaAs, CdTe, InSb, Si-on-insulator structures and metals. Since such a wide variety of materials is treated, details concerning laser–solid interactions in any single system are necessarily limited. Nevertheless, the chapter provides a good introduction to laser annealing and transient processing and offers an informative survey of work in this field.

The emphasis of the second chapter is on the photophysics and photochemistry of gas–surface interactions. Although this is a rela-

continued on page 409